IEEE Access
Multidisciplinary | Rapid Review | Open Access Journal

IEEE GEOSCIENCE AND REMOTE SENSING SOCIETY SECTION

Received 31 March 2024, accepted 8 April 2024, date of publication 15 April 2024, date of current version 22 April 2024.

Digital Object Identifier 10.1109/ACCESS.2024.3388431

RESEARCH ARTICLE

Application of Variational Bayesian Filtering Based on T-Distribution in BDS Dynamic Ambiguity Resolution

WEI CAI[1,2], YANG SHEN[1], MINGJIAN CHEN[1], WEI ZHOU[2], JING LI[2], JIANLUN HE[2], AND XIN JING[2]

[1]Institute of Geospatial Information, Information Engineering University, Zhengzhou 450001, China
[2]Xi'an Mapping Terminus, Xi'an 710054, China

Corresponding author: Yang Shen (sy665432@163.com)

This work was supported by the National Natural Science Foundation of China under Grant 42104034.

ABSTRACT In dynamic environments, the traditional relative positioning methods based on the Kalman filter model suffer from low accuracy and stability due to the influence of noise and outliers. This paper proposes a variational Bayesian filtering algorithm based on the combination of four-frequency observations from BDS (BeiDou Navigation Satellite System) and models the observation noise using the T-distribution to enhance the stability of filtering. Firstly, a geometrically correlated ambiguity resolution model is constructed based on the characteristics of the combined observations, effectively improving the precision of float ambiguity resolution and fixing rate. Moreover, considering the characteristics of outliers that are likely to occur in dynamic conditions, a T-distribution-based variational Bayesian filtering approach is employed to estimate the time-varying observation noise and system states. Experimental results demonstrate that the proposed method exhibits robustness and stability in dynamic short baseline scenarios, leading to further improvements in positioning accuracy, float ambiguity resolution precision, and fixing rate.

INDEX TERMS BeiDou navigation satellite system, ambiguity, variational Bayesian, T-distribution, short baseline.

I. INTRODUCTION

The primary approach to obtaining accurate positions of dynamic users is through dynamic relative positioning using carrier phase observations. The key challenge in achieving high-precision relative positioning results lies in rapidly resolving the correct integer ambiguities.

Currently, the BeiDou Navigation Satellite System (BDS-3) has been fully established, capable of broadcasting navigation signals on five frequencies, providing more accurate navigation and positioning services [1]. The most significant advantage of multi-frequency signals is to improve the success rate of integer ambiguity resolution. The linear combination of multiple frequencies can obtain high quality combined observations, which have the characteristics of long wavelength, small noise factor and ionospheric factor, and can basically realize the integer ambiguity fixed in a single epoch. Zhang used the real BDS-3 four-frequency data of short baseline and medium and long baseline for linear combination, and used two different methods of geometry-free model and geometric correlation to verify that compared with the traditional three-frequency, the number of combined observations is more and the quality is better, and the integer ambiguity can be fixed instants [2]. Currently, TCAR method based on BDS-2 for B1I, B2I and B3I signals is still the most common method for integer ambiguity resolution using BDS multi-frequency, where the wide-lane and narrow-lane ambiguities of BDS are successively fixed. However, as the baseline length increases, the influence of ionospheric and atmospheric delay errors increases, leading to lower fixing rates for narrow-lane ambiguities, Zhang used the B1I, B2I and B3I three-frequency signals of BDS-2, and used the TCAR method based on non-geometric model to solve the ambiguity in the order of ultra-wide lane ambiguity, wide lane

The associate editor coordinating the review of this manuscript and approving it for publication was Gerardo Di Martino.

ambiguity and narrow lane ambiguity. The effect of TCAR is verified by the data of CUTA and CUT2 stations with a baseline length of 8m in Cottdington, Australia, and JFEG and WHDH stations with a baseline length of 8.3km in Wuhan, respectively. The ultra-short baseline with a baseline length of 8m has a narrow-lane ambiguity fixed rate of 100%. For the short baseline length of 8.3km, the fixed rate of narrow lane ambiguity is only 53.5% [3]. Gao et al. [4] from the Information Engineering University proposed an improved TCAR algorithm that considers the effects of ionospheric delay and observation noise, achieving correct ambiguity fixing in medium-to-long baselines with good adaptive robustness, with a narrow-lane ambiguity fixing rate of around 80%. Subsequently, Li et al. [5] conducted in-depth research on Multi-frequency Carrier Ambiguity Resolution (MCAR) using the five-frequency signals broadcasted by BDS-3. It was found that linear combinations of observations from four frequency points can construct combined observations with weak ionospheric delay and minimal observation noise, effectively improving the ambiguity fixing rate. Researchers at home and abroad have conducted studies on relative positioning using four-frequency combined observations. Liu et al. [6] made full use of the four BDS frequencies, linearly combined them, selected the optimal combined observations, and used the non-geometric phase pseudo-range and geometric correlation model to resolve the ambiguities in a single epoch. In short-baseline scenarios, this method can achieve single-epoch fixing of wide-lane and narrow-lane ambiguities, with a narrow-lane ambiguity fixing rate exceeding 99% and positioning accuracy reaching centimeter-level. Cao et al. [7] used weak ionospheric combinations composed of BDS-3 four frequencies in medium-to-long baselines. By considering the influence of tropospheric delay errors and establishing a medium-to-long baseline solution model, the ambiguity fixing rate increased by more than 10% compared to the traditional dual-frequency non-ionospheric combination, and the three-dimensional coordinate positioning accuracy improved by about 8%. In summary, four-frequency combined observations can improve the ambiguity fixing rate and solution efficiency for baselines of various lengths.

Currently, in the dynamic environment, the primary solution is to shorten the initialization time of ambiguity and improve the reliability of ambiguity resolution. The general method is to reduce the search space of ambiguity by adding redundant observations or improving the accuracy of redundant observations, so as to speed up the ambiguity fixation and improve the reliability of ambiguity resolution, Lv et al. [8] used the four-frequency signal of BDS-3 to construct the positioning equation by combining the ionospheric elimination combination and the combined observation values of three ultra-wide lanes with fixed ambiguity. In the positioning solution of the 500km long baseline, the ambiguity fixation rate of the narrow lane increased by about 1%, and the positioning accuracy of the horizontal direction and vertical direction increased by 35% and 40%. Geng et al. [9] used 31 days of three-frequency multi-GNSS data from 76 stations in Asia and Oceania, replaced the pseudo-range observation values of ultra-wide lane and wide lane with fixed ambiguity, improved the convergence of narrow lane ambiguity, and shortened the average initialization time of narrow lane by 3 minutes. Liu et al. [10] respectively used two four-frequency high-quality ultra-wide lane combined observations of BDS-3 and Galileo with fixed ambiguity to constrain the solution of wide lane ambiguity, and increased the precision of floating point solution of wide lane ambiguity. At present, the relative positioning under dynamic conditions mostly uses the combination of three frequency signals, and four frequency signals can form more high-quality combined observations than three frequency signals. However, there are few researches on dynamic relative positioning using the combination of four frequency signals. In order to adapt to the more complex dynamic environment, the redundant observations with high precision are added, so as to improve the efficiency, accuracy and reliability of ambiguity resolution, this paper adopts a four-frequency signal geometric-based (GB) solution model of ''wide-lane + narrow-lane + narrow-lane''. The conventional geometric correlation model aims to resolve each type of ambiguity through least squares, as demonstrated in [8]. In contrast, the solution model proposed in this paper addresses the ultra-wide lane ambiguity first using a combination of Kalman filter and LAMBDA algorithm, followed by wide lane ambiguity and narrow lane ambiguity. Specifically, at each epoch, the ultra-wide lane ambiguity is initially estimated via filtering. Subsequently, it is directly incorporated into the observation equation for wide lane to resolve the wide lane ambiguity. Finally, the obtained wide lane ambiguity are transferred to the observation equation for narrow lane to solve the narrow lane ambiguity. In practical environments, moving carrier positioning will be affected by various noise, signal occlusion and multipath effect, electromagnetic interference, dynamic stress and vibration, satellite signal problems and other factors, leading to the occurrence of outliers in observation noise, and the distribution of observation noise no longer exhibits Gaussian characteristics but exhibits heavy-tailed characteristics. The traditional relative positioning model is solved by Kalman filter model based on Gaussian distribution, such as open source software Rtklib, whose noise model is set to Gaussian white noise, and can not deal with the problem of time-varying noise variance of the model. However, directly applying Kalman filtering in the presence of outliers in observation noise will result in reduced filtering performance and decreased accuracy. Since the T-distribution has heavy-tailed characteristics compared to the Gaussian distribution, approximating the observation noise with a T-distribution can improve filtering performance [11]. To adapt to the interference of dynamic environments, the traditional Gaussian white noise model in this paper is replaced with the T distribution, and the Kalman filter algorithm is modified to incorporate the Variational Bayesian algorithm. This adaptation enables real-time

estimation of statistical characteristics of measured noise and adaptive approximation of the true posterior distribution. Finally, the ambiguity fixing rate and baseline solution accuracy of the dynamic positioning method are analyzed through experiments.

II. LINEAR COMBINATION OF BDS MULTI-FREQUENCY SIGNALS

Using the pseudorange and phase signals from the B1I, B1C, B3I, and B2a frequencies of BDS-3, linear combinations can be formed to create combined observations with different wavelengths, ionospheric delay amplification factors, observation noise amplification factors, and overall noise levels. Typically, combination coefficients with longer wavelengths, weaker ionospheric delay effects, and smaller observation noise are selected to obtain high-quality combined observations. However, there are few combinations that simultaneously satisfy these conditions among the available coefficient options. Therefore, the concept of overall noise level is introduced to determine the optimal combination coefficients. This approach considers not only ionospheric delay errors and observation noise but also orbital errors and tropospheric delay errors. The expressions for the overall noise levels of pseudorange and phase are as follows:

$$\delta_\varphi = \frac{1}{\lambda_{(k,l,m,n)}}\sqrt{\delta_{orb}^2 + \delta_{trop}^2 + \mu_{(k,l,m,n)}^2\delta_I^2 + \eta_{(k,l,m,n)}^2\varepsilon_\varphi^2} \quad (1)$$

$$\delta_p = \sqrt{\delta_{orb}^2 + \delta_{trop}^2 + \mu_{(a,b,c,d)}^2\delta_I^2 + \eta_{(a,b,c,d)}^2\varepsilon_p^2} \quad (2)$$

In the expressions, the overall noise level of phase and pseudorange observations is δ_φ, δ_p given in units of cycles and meters, respectively. The orbital error is δ_{orb}, tropospheric delay error is δ_{trop}, first-order ionospheric delay error is δ_I, observation noise of carrier phase and pseudorange are ε_φ, ε_p, combined wavelength is $\lambda_{(k,l,m,n)}$, combination coefficients for phase and pseudorange are k, l, m, n, a, b, c, d, ionospheric delay amplification factor is $\mu_{(k,l,m,n)}$, and observation noise amplification factor is $\eta_{(k,l,m,n)}$. The expressions of$\mu_{(k,l,m,n)}$, $\lambda_{(k,l,m,n)}$are as follows [6]:

$$\mu_{(k,l,m,n)} = \frac{f_1^2}{kf_1 + lf_2 + mf_3 + nf_4}\left(\frac{k}{f_1} + \frac{l}{f_2} + \frac{m}{f_3} + \frac{n}{f_4}\right) \quad (3)$$

$$f_{(k,l,m,n)} = k\cdot f_1 + l\cdot f_2 + m\cdot f_3 + n\cdot f_4 \quad (4)$$

$$\lambda_{(k,l,m,n)} = c/f_{(k,l,m,n)} \quad (5)$$

In the expressions, $f_1 \sim f_4$ represents the four frequencies, $f_{(k,l,m,n)}$ represents the combined frequency, c represents the speed of light in vacuum. The expression for the ionospheric delay amplification factor of pseudorange is similar, except for the different combination coefficients. Let $\delta_{\varepsilon_\varphi}^2$ and $\delta_{\varepsilon_p}^2$ represent the observation noise precision for phase and pseudorange, respectively. According to literature [7], the noise of carrier phase observations at each frequency is the same, and the noise of pseudo-distance observations is the same, $\delta_{\varepsilon\varphi 1} = \delta_{\varepsilon\varphi 2} = \delta_{\varepsilon\varphi 3} = \delta_{\varepsilon\varphi 4} = \delta_{\varepsilon\varphi}, \delta_{\varepsilon P1} = \delta_{\varepsilon P2} = \delta_{\varepsilon P3} = \delta_{\varepsilon P4} = \delta_{\varepsilon P}$, the expressions of $\delta_{\varepsilon_\varphi}^2, \delta_{\varepsilon_p}^2$ are as follows [6]:

$$\delta_{\varepsilon_\varphi}^2 = \eta_{(k,l,m,n)}^2\cdot\varepsilon_\varphi^2 \quad (6)$$

$$\delta_{\varepsilon_p}^2 = \eta_{(a,b,c,d)}^2\cdot\varepsilon_p^2 \quad (7)$$

the expression of $\eta_{(k,l,m,n)}$ is as follows [6]:

$$\eta_{(k,l,m,n)} = \sqrt{\frac{(kf_1)^2 + (lf_2)^2 + (mf_3)^2 + (nf_4)^2}{f_{(k,l,m,n)}^2}} \quad (8)$$

When δ_φ, δ_p is minimized, the coefficients in equation (6) and (7) are satisfied $(kf_1)^2 + (lf_2)^2 + (mf_3)^2 + (nf_4)^2 = \min k + l + m + n = 0, a + b + c + d = 1$, the combination coefficients are optimal [12]. For medium-length baselines (length $\leq$ 100 km), according to references [6], the values of the error terms in the overall noise level are: 0.005 m, 0.01 m, 0.1 m, and 0.005 m. According to references [13], [14], the optimal combination coefficients for different wavelengths are categorized as wide-lane, medium-lane, and narrow-lane combinations, as shown in Table 1.

TABLE 1. BDS-3 four frequency optimal combination coefficient.

k	l	m	n	$\lambda_{(k,l,m,n)}$ /m	$\mu_{(k,l,m,n)}$ /m	$\eta_{(k,l,m,n)}$ /m	δ /cycle
0	0	1	-1	3.2561	-1.633	18.791	0.052
0	1	-3	2	2.4421	-0.599	38.640	0.160
1	0	-2	1	1.4952	-1.046	15.973	0.128
0	1	-1	0	0.9768	-1.2195	6.591	0.142
2	0	2	-3	0.1093	0.0049	2.066	0.14

The table presented in Table 1 provides the combination coefficients (k, l, m, and n) for the carrier phase of four frequencies. Although some coefficients are zero, all of their combinations cover all four frequencies. It is important to note that a single satellite transmission must include all four frequencies simultaneously. Hence, this table is referred to as the optimal four-frequency combination coefficient. Furthermore, λ represents the wavelength of the combined observation value which can be categorized into three categories according to wavelength: When $\lambda \geq 2.93m$, ultra-wide lane combination correspondence to (0, 0, 1,−1) in the table. When $0.75m \leq \lambda < 2.93m$, wide lane combination correspondence (0, 1,-2,1), (1,0,-2,1), (0,1,−1,0) in the table respectively. When $0.1m \leq \lambda < 0.75m$, narrow lane combination correspondence (2,0,2,−3) in the table. The table provide valuable information about ionospheric factors affecting combined observations; smaller values indicate lower ionospheric delay errors. Additionally, the table also account for noise factors influencing observed data quality. Smaller noise factors result in reduced observed noise levels. Lastly, total noise level considers both wavelength and ionospheric factor alongside noise factor. Lower total noise levels signify higher quality observed values with easier ambiguity resolution.

III. ULTRA WIDE-LANE/WIDE-LANE/NARROW-LANE AMBIGUITY RESOLUTION BASED ON THE GB MODEL

A. ULTRA WIDE-LANE AMBIGUITY FIXING

The Ultra wide-lane ambiguity resolution method based on the GB model involves combining a set of Ultra wide-lane

combination observations with the optimal combination of pseudorange observations. The three-dimensional coordinates and wide-lane ambiguities are the parameters to be estimated. The solution is obtained using Kalman filtering and the LAMBDA algorithm. The mathematical model for the solution is expressed as follows:

$$\begin{bmatrix} \boldsymbol{E} & \lambda_{(k_1,l_1,m_1,n_1)} \\ \boldsymbol{E} & \boldsymbol{0} \end{bmatrix} \begin{bmatrix} \boldsymbol{X}_r \\ \boldsymbol{N}_{(k_1,l_1,m_1,n_1)} \end{bmatrix} = \begin{bmatrix} \nabla\Delta\phi_{(k_1,l_1,m_1,n_1)} - \nabla\Delta\rho + \nabla\Delta I - \nabla\Delta T \\ \nabla\Delta P_{(a,b,c,d)} - \nabla\Delta\rho - \nabla\Delta I - \nabla\Delta T \end{bmatrix} \tag{9}$$

Here, $\begin{bmatrix} \boldsymbol{E} & \lambda_{(k_1,l_1,m_1,n_1)} \\ \boldsymbol{E} & \boldsymbol{0} \end{bmatrix}$ represents the linearized observation matrix in Kalman filter $\boldsymbol{E} = \begin{bmatrix} e^1 - e^2 & e^1 - e^3 & \cdots & e^1 - e^m \end{bmatrix}^T$ represents the direction cosine, where e^1 represents the reference star unit line of sight vector, $e^2 \cdots e^m$ represents the non-reference star unit line of sight vector; $\begin{bmatrix} \boldsymbol{X}_r \\ \boldsymbol{N}_{(k_1,l_1,m_1,n_1)} \end{bmatrix}$ represents state vector; $\begin{bmatrix} \nabla\Delta\phi_{(k_1,l_1,m_1,n_1)} - \nabla\Delta\rho + \nabla\Delta I - \nabla\Delta T \\ \nabla\Delta P_{(a,b,c,d)} - \nabla\Delta\rho - \nabla\Delta I - \nabla\Delta T \end{bmatrix}$ represents measure vector; $\boldsymbol{X}_r$ represents the three-dimensional coordinates of the moving station; $\boldsymbol{N}_{(k_1,l_1,m_1,n_1)}$ represents the Ultra wide-lane ambiguities; $\nabla\Delta\rho$ represents the geometric double-difference between the satellite and the receiver; $\nabla\Delta I$ represents the ionospheric delay double-difference corrected using the Klobuchar model and $\nabla\Delta T$ represents the tropospheric delay double-difference corrected using the Saastamoinen model. $\phi_{(k_1,l_1,m_1,n_1)}$ and $P_{(a,b,c,d)}$ represent the ombination observations of phase and pseudorange, respectively, and the expressions are as follows [6]:

$$\phi_{(k_1,l_1,m_1,n_1)} = \frac{k_1 f_1 \cdot \phi_1 + l_1 f_2 \cdot \phi_2 + m_1 f_3 \cdot \phi_3 + n_1 f_4 \cdot \phi_4}{k_1 f_1 + l_1 f_2 + m_1 f_3 + n_1 f_4} \tag{10}$$

$$P_{(a,b,c,d)} = \frac{a f_1 \cdot P_1 + b f_2 \cdot P_2 + c f_3 \cdot P_3 + d f_4 \cdot P_4}{a f_1 + b f_2 + c f_3 + d f_4} \tag{11}$$

Here, ϕ_1, ϕ_2, ϕ_3, ϕ_4 and P_1, P_2, P_3, P_4 represent the phase and pseudorange observations at the four frequency points, respectively. The wide-lane combination coefficients used in this study are (0,0,1,−1). Under the condition of pseudorange observation noise of 0.5 m, the standard selection of the optimal pseudorange combination coefficients is (1, 1, 1, 1).

At each epoch, the floating-point solution for the coordinate parameters and ambiguities is obtained using Kalman filtering. Then, the floating point solution and its corresponding variance-covariance matrix are substituted into the LAMBDA algorithm, and the integer solution of the ultra-wide lane is searched and fixed by the LAMBDA algorithm.

B. WIDE-LANE AMBIGUITY FIXING

The Ultra wide-lane ambiguities solved in the previous step are substituted back into the wide-lane observation equations to obtain the Ultra wide-lane observations $\hat{\phi}_{(0,0,1,-1)}$ with fixed ambiguities. The modified Ultra wide-lane observation equations, along with the wide-lane observation equations, are then combined. The three-dimensional coordinates and wide-lane ambiguities are the parameters to be estimated. The solution is obtained using Kalman filtering, followed by fixing the ambiguities using the LAMBDA algorithm. The mathematical model for the solution is expressed as follows:

$$\begin{bmatrix} \boldsymbol{E} & \lambda_{(k_2,l_2,m_2,n_2)} \\ \boldsymbol{E} & \boldsymbol{0} \end{bmatrix} \begin{bmatrix} \boldsymbol{X}_r \\ \boldsymbol{N}_{(k_2,l_2,m_2,n_2)} \end{bmatrix} = \begin{bmatrix} \nabla\Delta\phi_{(k_2,l_2,m_2,n_2)} - \nabla\Delta\rho + \nabla\Delta I - \nabla\Delta T \\ \nabla\Delta\hat{\phi}_{(0,0,1,-1)} - \nabla\Delta\rho + \nabla\Delta I - \nabla\Delta T \end{bmatrix} \tag{12}$$

Here, $\lambda_{(k_2,l_2,m_2,n_2)}$ represent the three wavelengths of combined wide-lane observations, respectively. $\boldsymbol{N}_{(k_2,l_2,m_2,n_2)}$ represent three kinds of floating-point solutions of wide-lane ambiguity, respectively. $\nabla\Delta\phi_{(k_2,l_2,m_2,n_2)}$ represent three kinds of wide-lane double-difference combination observation values, respectively. The observation value $\hat{\phi}_{(0,0,1,-1)}$ of ultra-wide lane with fixed ambiguity is simultaneously combined with the observation equation of wide lane combination (0,1, −3,2), (1,0, −2,1) and (0,1, −1,0) respectively, and the Kalman filter algorithm is used to obtain (0,1, −3,2), (1,0, −2,1) and (0,1,−1,0) three combinations of wide lane ambiguity floating-point solutions, and then the fixed solution of wide lane ambiguity is obtained by LAMBDA algorithm. Three combined wide-lane ambiguities(0,1, −3,2), (1,0, −2,1), (0,1, −1,0)can be found by adopting the mode. the modified wide-lane combination observation $\nabla\Delta\hat{\phi}_{(0,1,-3,2)}$, $\nabla\Delta\hat{\phi}_{(1,0,-2,1)}$ and $\nabla\Delta\hat{\phi}_{(0,1,-1,0)}$ can be derived.

C. NARROW-LANE AMBIGUITY FIXING

The narrow-lane ambiguity fixing method involves combining the modified wide-lane combination observation equations with the narrow-lane combination observation equations. The three-dimensional coordinates and narrow-lane ambiguities are the parameters to be estimated. The solution is obtained using Kalman filtering and the LAMBDA algorithm. The mathematical model for the solution is expressed as follows:

$$\begin{bmatrix} \boldsymbol{E} & \lambda_{(k_3,l_3,m_3,n_3)} \\ \boldsymbol{E} & \boldsymbol{0} \\ \boldsymbol{E} & \boldsymbol{0} \\ \boldsymbol{E} & \boldsymbol{0} \end{bmatrix} \begin{bmatrix} \mathbf{X}_r \\ \mathbf{N}_{(k_3,l_3,m_3,n_3)} \end{bmatrix} = \begin{bmatrix} \nabla\Delta\phi_{(k_3,l_3,m_3,n_3)} - \nabla\Delta\rho + \nabla\Delta I - \nabla\Delta T \\ \nabla\Delta\hat{\phi}_{(0,1,-3,2)} - \nabla\Delta\rho + \nabla\Delta I - \nabla\Delta T \\ \nabla\Delta\hat{\phi}_{(1,0,-2,1)} - \nabla\Delta\rho + \nabla\Delta I - \nabla\Delta T \\ \nabla\Delta\hat{\phi}_{(0,1,-1,0)} - \nabla\Delta\rho + \nabla\Delta I - \nabla\Delta T \end{bmatrix} \tag{13}$$

Here, $\lambda_{(k_3,l_3,m_3,n_3)}$ represents the wavelength of the combined observations of the narrow lane, respectively. $\boldsymbol{N}_{(k_3,l_3,m_3,n_3)}$ represents the floating-point solution of the narrow lane ambiguity. $\nabla\Delta\phi_{(k_3,l_3,m_3,n_3)}$ represent represents the combined observation of double difference in the narrow lane. The wide lane observation values $\nabla\Delta\hat{\phi}_{(0,1,-3,2)}$, $\nabla\Delta\hat{\phi}_{(1,0,-2,1)}$

TABLE 2. Solution strategy.

Project	Processing strategy
BDS-3 frequency	B1I、B1C、B3I、B2a
elmask	15°
Stochastic model	RTKLIB Empirical formula
Satellite ephemeris	Broadcast ephemeris
Ionospheric delay	**Klobuchar**
Tropospheric delay	**Saastamoinen**
Armode	Fix and hold
Ratio	3
Parameter estimation	Kalman filtering
Filter mode	Forward

and $\nabla\Delta\hat{\phi}_{(0,1,-1,0)}$ with fixed ambiguity are combined with the narrow lane observation equation, The Kalman filter algorithm is used to obtain the floating point solution of the narrow lane ambiguity, and then the fixed solution of the narrow lane ambiguity is obtained by the LAMBDA algorithm.

To verify the superiority of this model over the non-combination multi-frequency ambiguity fixing model in terms of ambiguity fixing rate and positioning accuracy, experiments were conducted using a set of medium-length baselines data within Henan Province. The baseline length was 62 km, the sampling interval was 1 second, and the data collection duration was 1 hour. The filtering method used was forward filtering, with a ratio set to 3 and a cutoff elevation angle set to 15°. Ratio represents the ratio of the optimal integer solution and the suboptimal integer solution of the LAMBDA search and represents the threshold of the ambiguity fixed solution. The empirical value is set to 3, and a ratio greater than or equal to 3 indicates that the optimal integer solution is a fixed solution. Due to the residual ionospheric delay error in the long baseline, which was not completely eliminated after double-difference correction, a weak ionosphere combination (2, 0, 2, −3) was used for the narrow-lane combination because table 1 shows that this combined observation has the smallest ionospheric factor and is affected by the least ionospheric delay. This model is based on modifications to the Rtklib software, and its data preprocessing and random model are the same as those of the Rtklib software. The results obtained using the two different methods were compared with the ground truth, as shown in Figures 1-3. The variation of the ratio which shows the degree of accuracy and reliability of the ambiguity fixed solution is shown in Figure 4. The number of effective common-view satellites obtained using the combination observation method is shown in Figure 5. The specific solution strategies are summarized in Table 2.

Based on Figure 1 to Figure 4, it can be observed that the positioning accuracy and ambiguity fixing rate are higher when using the GB four-frequency combination solving model. By comparing Figure 4 and Figure 5, it can be seen that at epoch 1335, the addition of new satellites in the

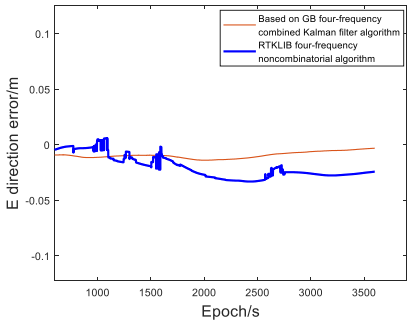

FIGURE 1. Based on GB four-frequency combined observations /Rtklib four-frequency uncombined algorithm and the difference between the true value in the E direction.

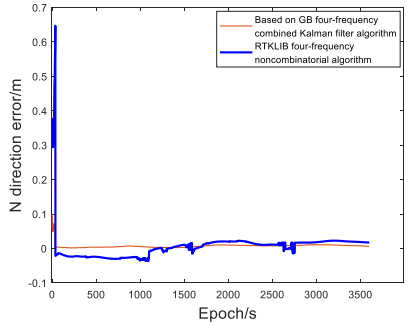

FIGURE 2. Based on GB four-frequency combined observations /Rtklib four-frequency uncombined algorithm and the difference between the true value in the N direction.

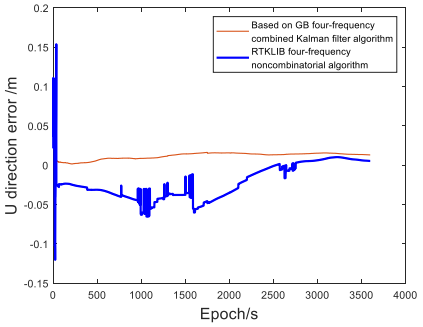

FIGURE 3. Based on GB four-frequency combined observations /Rtklib four-frequency uncombined algorithm and the difference between the true value in the U direction.

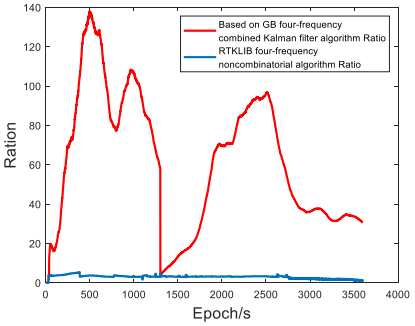

FIGURE 4. Ratio change based on GB four-frequency combination observation algorithm.

calculation significantly reduces the Ratio, this is because when a new satellite joins, the receiver needs to re-search and determine the integer ambiguity of the new satellite because

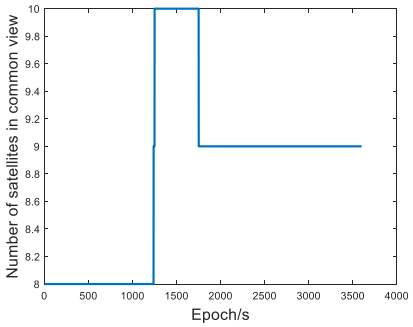

FIGURE 5. The number of effective co-visible satellite based on GB four-frequency combined observation algorithm.

TABLE 3. The results of the two algorithms are compared.

Algorithm	E direction error /m	N direction error /m	U direction error /m	Ambiguity fixed rate	The number of epoch required for ambiguity to be fixed for the first time
Based on GB four-frequency combined Kalman filter algorithm	0.0037	0.006	0.0084	99.2%	30
RTKLIB four-frequency noncombinatorial algorithm	0.019	0.0459	0.0377	98.1%	68

the position and signal characteristics of the new satellite are different from those of the original satellite. Specific statistical data can be found in Table 3.

In Table 3, the position error represents the results obtained by comparing the float solution and the fixed solution with the true values. The ambiguity fixing rate is obtained by comparing the number of epochs with fixed ambiguities to the total number of epochs involved in the calculation. According to Table 3, the GB four-frequency combination model, which utilizes three sets of wide-lane combination observations with higher accuracy compared to pseudorange observations, as redundant measurements to constrain the narrow-lane ambiguity resolution, achieves higher ambiguity fixing rate, less initialization time, and positioning accuracy than the non-combination solving model. After comparison, the positioning accuracy (Root mean square error) in the East (E), North (N), and Up (U) directions improves by 80.5%, 86.9%, and 77.7% respectively. The ambiguity fixing rate increases by 1.1%, and the initialization time of ambiguity is reduced by 55.9%. Generally, a higher Ratio indicates greater reliability of the ambiguity resolution, when the Ratio value is large, it means that the optimal solution has a more obvious advantage over the suboptimal solution, so the integer ambiguity resolution result is more reliable. On the contrary, if the Ratio value is small, it indicates that there is little difference between the optimal solution and the suboptimal solution, and there may be large error or uncertainty in the solution result of integer ambiguity. The change in Ratio shown in Figure 4 indicates that about 99% of the Ratio values of the two methods are greater than 3, indicating that the ambiguity fixation rate is high. Through the trend of the Ratio value, two new stars are added at epoch 1355, which leads to the ambiguity need to be fixed again and the Ratio value is reduced. At the same time, it can be seen that the Ratio value of the GB four-frequency combination model is larger than that of the non-combination solution model, which means the GB four-frequency combination model has higher reliability in ambiguity resolution compared to the non-combination solving model, so the positioning accuracy is higher.

IV. NARROW-LANE AMBIGUITY RESOLUTION UNDER DYNAMIC CONDITIONS

Based on the experimental analysis in Section II, it is known that using the GB four-frequency combination model allows for fast and reliable resolution of narrow-lane ambiguities. This model can be applied to dynamic ambiguity resolution.

In static conditions, most ambiguity resolution methods are based on the Kalman filtering algorithm, where the noise parameters are set empirically and kept fixed for superior performance [15], [16], [17]. However, in real-world environments, the noise may not necessarily follow the characteristics of Gaussian white noise. Modeling the noise based solely on Gaussian white noise assumptions has its limitations. When the target is in motion, the observation noise varies over time, and outliers may occur during the observation process. The actual noise distribution often exhibits heavy-tailed characteristics compared to a Gaussian distribution. The T-Distribution function, which has heavy-tailed properties, reduces sensitivity to outliers during the filtering process. By modeling the observation noise using T-Distribution function and combining it with variational Bayesian filtering methods, the statistical characteristics of the measurement noise can be adaptively estimated in real-time.

The T-Distribution function is expressed as follows:

$$p(v_k) = St(v_k; 0, \boldsymbol{R}_k, v) = \int N(v_k; 0, \frac{\boldsymbol{R}_k}{\lambda_k}) G(\lambda_k; \frac{v}{2}, \frac{v}{2}) d\lambda_k \tag{14}$$

In the equation, $St(v_k; 0, \boldsymbol{R}_k, v)$ represents the probability density function of T-Distribution with mean 0, scale matrix $\boldsymbol{R}_k$ and degrees of freedom v. When $v \to \infty$, the distribution is equivalent to a Gaussian distribution, making T-Distribution a mixture of Gaussians [19]. $G(\lambda_k; v/2, v/2)$ represents a gamma distribution with shape parameter $v/2$ and scale parameter $v/2.\lambda_k$ is an auxiliary random variable, and the measurement covariance matrix under the T-Distribution is denoted as $\boldsymbol{R}_k/\lambda_k$. To adaptively estimate the time-varying measurement noise, it is necessary to select a prior distribution for the time-varying parameters and then update the posterior information using variational Bayesian estimation. According to Equation (14), the auxiliary random variable and the degree of freedom parameter are treated as

a continuous parameter in the Bayesian estimation. so the prior distributions for the auxiliary random variable and the degrees of freedom parameter are gamma distributions, a common practice in Bayesian estimation is to choose the distribution of the variance as an inverse gamma distribution [19] while the inverse gamma distribution is selected as the prior distribution for the scale matrix. Based on the choice of prior distributions, the following formulas can be derived:

$$p(v) = Gamma(v; a_k, b_k) \tag{15}$$
$$p(\lambda_k) = Gamma(\lambda_k; \alpha_k, \beta_k) \tag{16}$$
$$p(\boldsymbol{R}_k) = \prod_{i=1}^{m} InvGamma(\delta_{k,i}^2 | c_{k,i}, d_{k,i}) \tag{17}$$

In the equation, $\delta_{k,i}^2$ represents the diagonal elements of the measurement noise covariance matrix, and m represents the dimension of the measurement vector. Using the Kalman filtering algorithm, it can be derived that the state vector follows a normal distribution $N(\boldsymbol{X}_k|\hat{\boldsymbol{X}}_{k,k-1}, \boldsymbol{P}_k^-)$, and the measurement vector follows a T-Distribution $St(\boldsymbol{Z}_k|\boldsymbol{H}_k\hat{\boldsymbol{X}}_{k,k-1}, \boldsymbol{R}_k, v)$.

The meanings of the symbols in the above expressions are as follows: $\boldsymbol{X}_{k-1}$ represents the state vector at time step k-1, $\boldsymbol{P}_{k-1}$ represents the state covariance matrix, the predicted expressions for the state vector and covariance at time step k is expressed as follows:

$$\hat{\boldsymbol{X}}_{k,k-1} = \boldsymbol{\Phi}_{k,k-1}\boldsymbol{X}_{k-1} \tag{18}$$
$$\boldsymbol{P}_k^- = \boldsymbol{\Phi}_{k,k-1}\boldsymbol{P}_{k-1}\boldsymbol{\Phi}_{k,k-1}^T + \boldsymbol{Q}_{k-1} \tag{19}$$

In the equation, $\boldsymbol{Q}_{k-1}$ represents the system noise variance matrix. The state estimation of Kalman filtering algorithm are expressed as follows.

$$\boldsymbol{K}_k = \boldsymbol{P}_k^-\boldsymbol{H}_k^T(\boldsymbol{H}_k\boldsymbol{P}_k^-\boldsymbol{H}_k^T + \boldsymbol{R}_k)^{-1} \tag{20}$$
$$\hat{\boldsymbol{X}}_k = \hat{\boldsymbol{X}}_{k,k-1} + \boldsymbol{K}_k(\boldsymbol{Z}_k - \boldsymbol{H}_k\hat{\boldsymbol{X}}_{k,k-1}) \tag{21}$$
$$\boldsymbol{P}_k = \boldsymbol{P}_k^- - \boldsymbol{K}_k\boldsymbol{H}_k\boldsymbol{P}_k^- \tag{22}$$

In the equation, $\boldsymbol{K}_k$ represents filter gain matrix.

According to equation (15)(16)(17) and joint probability density function of the measurement vector $\boldsymbol{Z}_k$ is expressed as follows:

$$\begin{aligned} &p(\Theta, \boldsymbol{Z}_{1:k}) \\ &\approx N(\boldsymbol{X}_k|\hat{\boldsymbol{X}}_{k,k-1}, \boldsymbol{P}_k^-)Gamma(\lambda_k|\frac{v}{2}, \frac{v}{2}) \\ &\times N(\boldsymbol{Z}_k|\boldsymbol{H}_k\boldsymbol{X}_k, \frac{\boldsymbol{R}_k}{u_k})\prod_{i=1}^{m} InvGamma(\delta_{k,i}^2|c_{k,i}, d_{k,i}) \end{aligned} \tag{23}$$

In the equation, Θ represents the set of parameters to be estimated, including v, λ_k, $\boldsymbol{X}_k$ and $\boldsymbol{R}_k$. The principle of variational Bayesian is to update the distribution parameter a_k, b_k, α_k, β_k, $c_{k,i}$, $d_{k,i}$ iteratively according to the prior distribution and measurement information. So the joint posterior probability density function of each parameter expressed as follows:

$$p(\Theta|\boldsymbol{Z}_{1:k}) \approx\sim q(\mathbf{X}_k)q(\boldsymbol{R}_k)q(\lambda_k)q(v) \tag{24}$$

The variational Bayesian method aims to approximate the true joint posterior distribution by minimizing the Kullback-Leibler (KL) divergence between two distributions. KL divergence is a commonly used metric to evaluate the difference between probability distributions. In Bayesian estimation, it is usually calculated by variational method. Variational method is the core of approximate parameter posterior calculation in variational Bayesian method. Then, the posterior approximation of the parameters is used as the prior information of the next filtering time, and the iterative update is performed to realize the purpose of adaptive estimation of the statistical characteristics of the parameters. By minimizing the KL divergence between the true posterior distribution and the approximate posterior distribution, the parameter estimation expressions can be obtained when the KL divergence reaches its minimum value of 0. The parameter estimation expressions are as follows [20], [21], (25)–(29), as shown at the bottom of the next page:

In the equation, α represents parameter shape parameter of gamma distributions, β represents parameter scale parameter of gamma distributions, m represents the dimension of the measurement, λ represents degrees of freedom, C is constant, the integral value for constraint $q(\lambda_k)$ is 1.

Because measurement noise modeled as T-Distribution, its covariance matrix $\hat{\boldsymbol{R}}_k$ is quotient of scale matrix $\boldsymbol{R}_k$ and auxiliary variable λ_k. the expression as follows:

$$\sum \hat{\boldsymbol{R}}_k^{i+1} = \frac{E^{i+1}[\boldsymbol{R}_k]}{E^{i+1}[\lambda_k]} \tag{30}$$

After multiple iterations of the filter, the floating-point solutions for the coordinate parameters and ambiguities of each epoch are estimated. Then, the LAMBDA algorithm [22] is used to search and fix the narrow-lane ambiguities. The fixed narrow-lane ambiguities are then substituted back into the narrow-lane combination observation equation, resulting in the fixed solution for the position coordinates. The entire algorithm process is illustrated in Figure 6.

V. EXPERIMENTAL ANALYSIS

To validate the feasibility of the proposed algorithm, dynamic data was collected on June 2, 2023, at the playground of the University of Information Engineering. The data collection involved attaching a SIRIUS receiver to an electric vehicle, which circled the playground. Network RTK mode was enabled, and the post-processed results were used as ground truth. The sampling interval was set to 1 second, and the data collection lasted approximately 40 minutes. According to the information in the observation file, the device can receive data continuously during dynamic acquisition, the integrity of data can be guaranteed in each epoch, the carrier phase and pseudorange of each frequency are complete, and the number of satellites can meet the positioning solution.

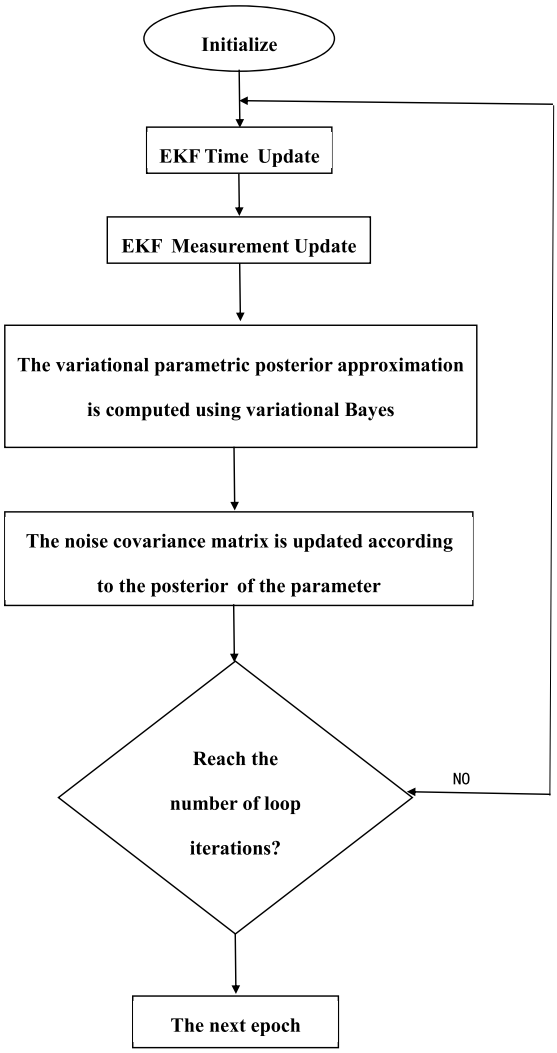

FIGURE 6. Flow chart of variational Bayesian EKF algorithm based on T distribution.

The reference station was located on the roof of a teaching building, and its position was obtained using network RTK. The distance between the reference station and the moving station was around 300 meters. Due to the short baseline

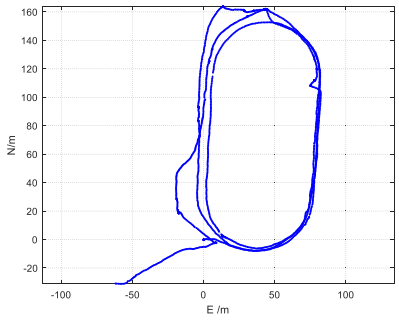

FIGURE 7. Dynamic experimental trajectory.

in the experiment, the narrow-lane combination was set to (1,0,0,0) to reduce the impact of observation noise. The wide-lane combinations used were (0,1,−3,2), (1,0,-2,1), and (0,1,−1,0). The motion trajectory is shown in Figure 7, and the programs were implemented based on Rtklib. The only modification made was the change of the positioning mode to dynamic, while the filtering models were either Kalman filter or variational Bayesian filter. The other positioning strategies followed the ones listed in Table 2.

To validate the superiority of the four-frequency combined ambiguity resolution model over the four-frequency non-combined and three-frequency combined ambiguity resolution models, the results obtained from the four-frequency combined Kalman filter algorithm were compared with those from the four-frequency non-combined and three-frequency combined algorithms. Additionally, to verify the improved performance of the variational Bayesian filter based on the T-distribution over the traditional Kalman filter under dynamic conditions, the results obtained from the four-frequency combined variational Bayesian filter based on the T-distribution were compared with those from the four-frequency combined Kalman filter.

The comparison between the results obtained from the four-frequency combined observations using the Kalman filter and the results obtained from the four-frequency non-combined observations using the Kalman filter is shown in Figures 8-10. The comparison between the results

$$\ln q(\lambda_k) = -\frac{v + tr(\boldsymbol{R}_k(\boldsymbol{H}_k\boldsymbol{P}_k\boldsymbol{H}_k^T + (\boldsymbol{Z}_k - \boldsymbol{H}_k\hat{\boldsymbol{X}}_k)^T \times (\boldsymbol{Z}_k - \boldsymbol{H}_k\hat{\boldsymbol{X}}_k)))}{2}\lambda_k + (\frac{m+v}{2} - 1)\ln\lambda_k + C \tag{25}$$

$$q(\lambda_k) = Gamma(\lambda_k|\alpha, \beta)$$

$$\alpha = \frac{m+v}{2} \tag{26}$$

$$\beta = \frac{tr(\boldsymbol{R}_k(\boldsymbol{H}_k\boldsymbol{P}_k\boldsymbol{H}_k^T + (\boldsymbol{Z}_k - \boldsymbol{H}_k\hat{\boldsymbol{X}}_k)^T \times (\boldsymbol{Z}_k - \boldsymbol{H}_k\hat{\boldsymbol{X}}_k))) + v}{2} \tag{27}$$

$$q(\boldsymbol{X}_k) = \frac{1}{C}N(\boldsymbol{Z}_k|\boldsymbol{H}_k\boldsymbol{X}_k, \frac{\boldsymbol{R}_k}{E(\lambda_k)})N(\boldsymbol{X}_k|\hat{\boldsymbol{X}}_{k,k-1}, \boldsymbol{P}_k^-) \tag{28}$$

$$\boldsymbol{K}_k = \boldsymbol{P}_k^-\boldsymbol{H}_k^T(\boldsymbol{H}_k\boldsymbol{P}_k^-\boldsymbol{H}_k^T + \frac{\boldsymbol{R}_k}{E(\lambda_k)})^{-1} \tag{29}$$

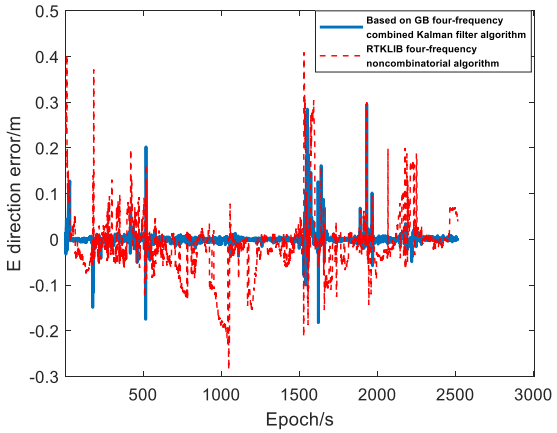

FIGURE 8. Deviation from the true value in the E direction of the Kalman filter solution results of the four-frequency combined observations and the non-combined observations.

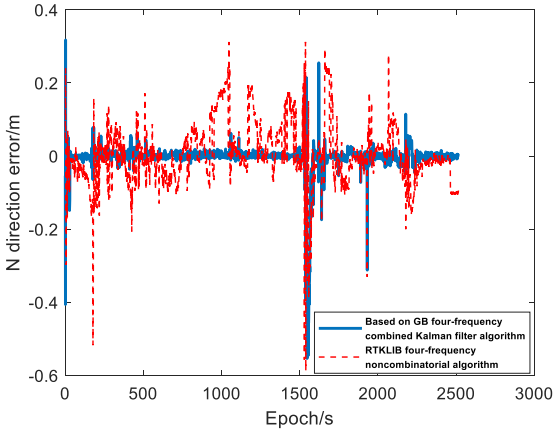

FIGURE 9. Deviation from the true value in the N direction of the Kalman filter solution results of the four-frequency combined observations and the non-combined observations.

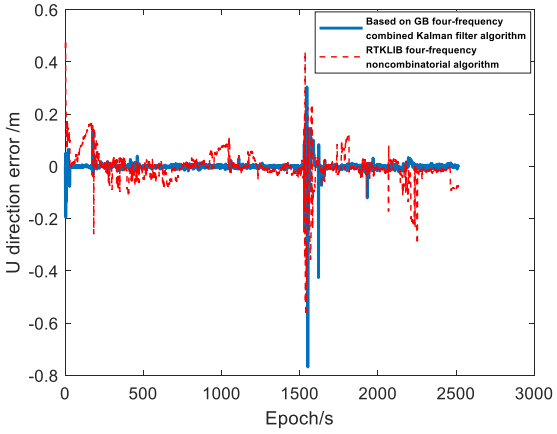

FIGURE 10. Deviation from the true value in the U direction of the Kalman filter solution results of the four-frequency combined observations and the non-combined observations.

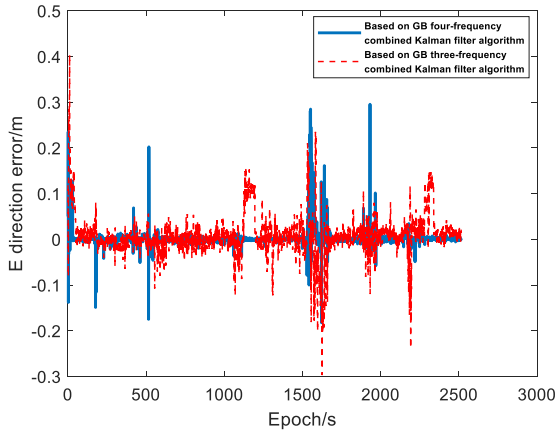

FIGURE 11. Deviation from the true value in the E direction of the Kalman filter solution results of the four-frequency combined observations and the three-frequency combined observations.

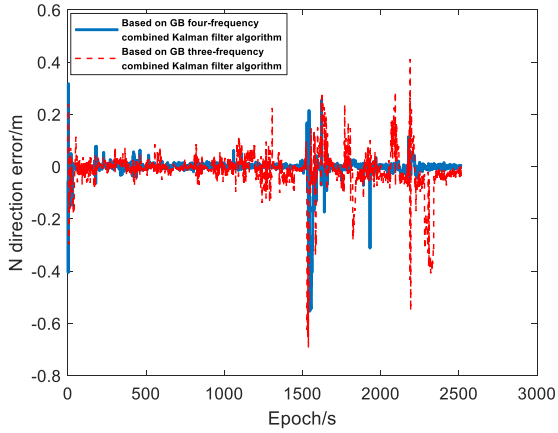

FIGURE 12. Deviation from the true value in the N direction of the Kalman filter solution results of the four-frequency combined observations and the three-frequency combined observations.

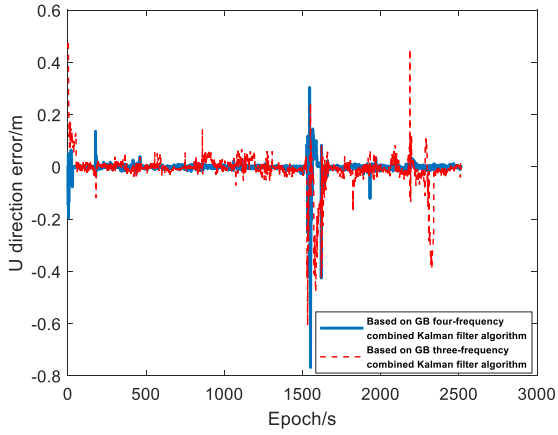

FIGURE 13. Deviation from the true value in the U direction of the Kalman filter solution results of the four-frequency combined observations and the three-frequency combined observations.

obtained from the four-frequency combined observations using the Kalman filter and the results obtained from the three-frequency combined observations using the Kalman filter is shown in Figures 11-13. The comparison between the results obtained from the four-frequency combined observations using the Kalman filter and the results obtained from the variational Bayesian filter based on the T-distribution is shown in Figures 14-16. The number of effective satellite co-observations for the four-frequency combined observations is shown in Figure 17, and the Ratio values of the ambiguity resolution obtained using the variational Bayesian filter based on the T-distribution are shown in Figure 18.

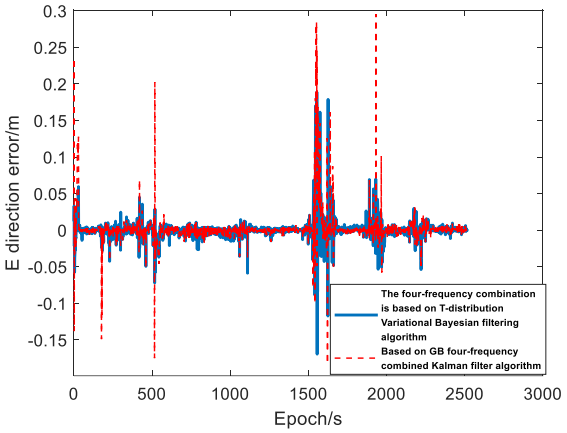

FIGURE 14. Deviation from the true value in the E direction of the solution results of the four-frequency combined observation Kalman filter and the T-distribution Bayesian filter.

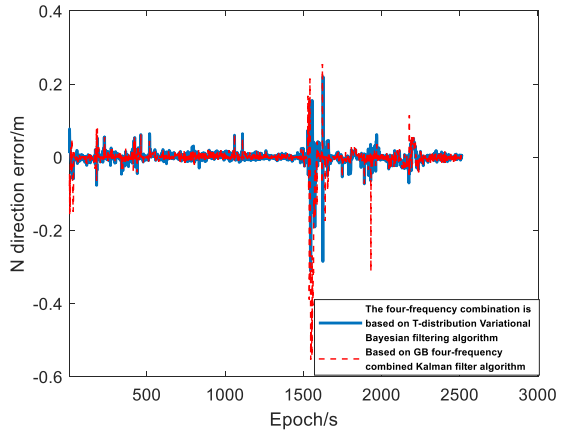

FIGURE 15. Deviation from the true value in the N direction of the solution results of the four-frequency combined observation Kalman filter and the T-distribution Bayesian filter.

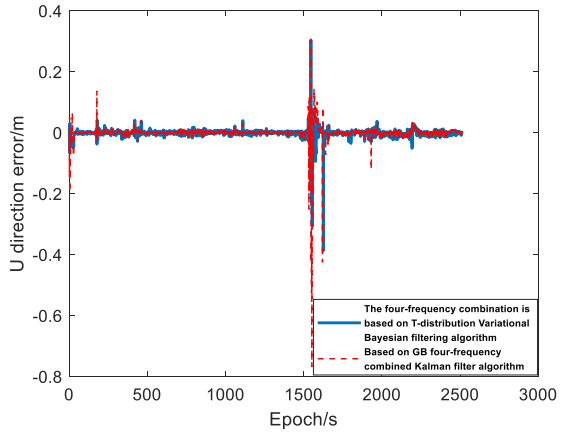

FIGURE 16. Deviation from the true value in the U direction of the solution results of the four-frequency combined observation Kalman filter and the T-distribution Bayesian filter.

From Figures 8-10, it can be observed that when employing the Kalman filter, the algorithm utilizing four-frequency combined observations achieves superior positioning accuracy and ambiguity fixing rate compared to the algorithm using non-combined observations. The three-dimensional

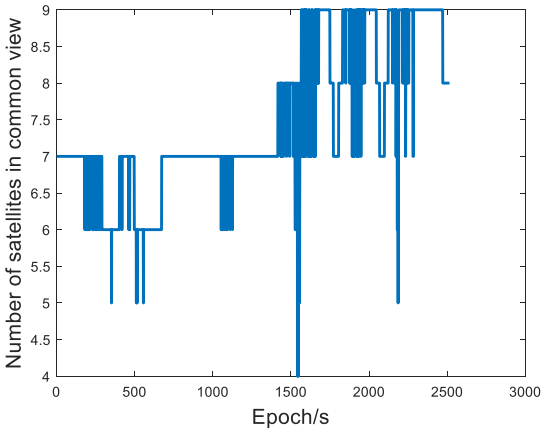

FIGURE 17. The number of co-looking satellites satisfying the four-frequency combined observations solution model.

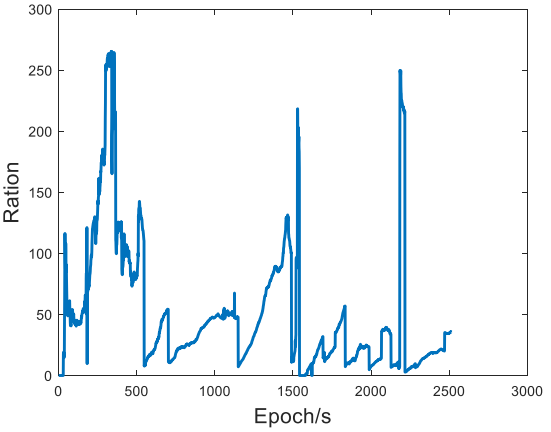

FIGURE 18. Ratio change of ambiguity resolution based on T-distribution Bayesian filtering.

coordinate accuracy (Root mean square error) is improved by 66.2%, 46%, and 52.2% respectively, while the ambiguity fixing rate is increased by 24.4%. From Figures 11-13, it is evident that as the number of frequencies increases, the algorithm based on four-frequency combined observations outperforms the algorithm based on three-frequency combined observations in terms of positioning accuracy. The three-dimensional coordinate accuracy (Root mean square error) is improved by 48.9%, 41.9%, and 52.2% respectively, while the ambiguity fixing rate is increased by 5.2%. From Figures 14-16, it can be observed that the variational Bayesian filter based on the T-distribution achieves higher accuracy than the Kalman filter algorithm. Figures 17-18 demonstrate that during the ambiguity resolution process using the variational Bayesian filter based on the T-distribution, the Ratio values fluctuate with changes in the number of satellites. Except for the initial stage of the resolution process where the Ratio value is below the threshold of 3, and during significant fluctuations in the number of satellites (3-4 satellites), the Ratio value is also below 3. However, overall, the majority of Ratio values exceed 3, reaching 96.9%, it means that only the Ratio value greater than 3 indicates that the ambiguity can be fixed solution, indicating that the ambiguity fixed rate reaches 96.9%. The high ambiguity fixing rate indicates

TABLE 4. Comparison of the solution results of different algorithms.

Algorithm	E direction error /m	N direction error /m	U direction error /m	Ambiguity fixed rate
The four-frequency combination is based on T-distribution Variational Bayesian filtering algorithm	0.014	0.021	0.019	96.9%
Based on GB four-frequency combined Kalman filter algorithm	0.024	0.047	0.032	93.2%
Based on GB three-frequency combined Kalman filter algorithm	0.047	0.081	0.067	88%
RTKLIB four-frequency noncombinatorial algorithm	0.071	0.087	0.067	68.8%

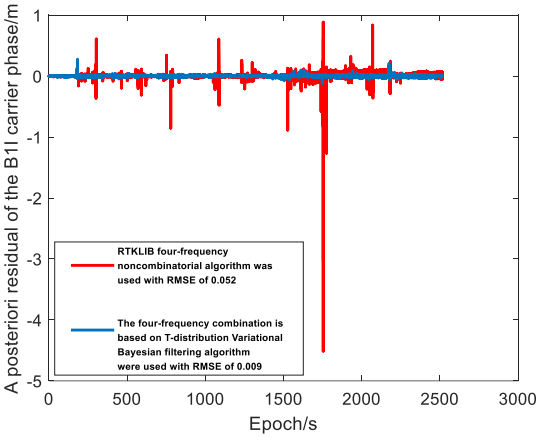

FIGURE 19. The post-test residual of carrier phase obtained by two different solutions.

superior positioning accuracy compared to the Kalman filter algorithm. The statistical results of positioning accuracy and ambiguity fixing rate in the East (E), North (N), and Up (U) components using different methods are summarized in Table 4.

To further illustrate the suitability of the variational Bayesian filter based on the T-distribution for positioning estimation in dynamic environments, the algorithm proposed in this paper verifies the posterior residuals of carrier phase measurements. Specifically, the final estimation in this algorithm is the carrier phase of the B1I signal from BDS-3 satellites. To compare the performance of the filtering models, the original Rtklib software based on the Kalman filter model was used to compute the four-frequency signals of BDS-3. The posterior residuals of the carrier phase measurements for the B1I signal were then used as the reference for comparison. The comparison results are shown in Figure 19.

From Figure 19, it can be observed that the posterior residuals of the B1I carrier phase estimated using the variational Bayesian filter based on the T-distribution are smaller. The error is 0.009m, which is 84.6% smaller than the values computed by the Rtklib software. Smaller residuals indicate that the proposed estimation model better matches the current motion state.

VI. CONCLUSION

In real-world scenarios, whether it is vehicle positioning during driving or drone positioning during flight, the satellite signals observed by the positioning receivers on the moving platforms frequently experience signal loss and outliers, which can significantly degrade the efficiency and reliability of ambiguity resolution in the positioning estimation process. Moreover, under dynamic conditions, the distribution of observation noise deviates from the Gaussian distribution. If the traditional Kalman filter algorithm based on the non-combined observation double-difference model is used in such situations, the efficiency and accuracy of ambiguity resolution will be greatly reduced.

To address this issue, this study proposes a four-frequency signal integration model, combining narrow-lane, ultra-wide-lane, and wide-lane observations, with both geometric and non-geometric approaches. Compared to the traditional non-geometric model, this approach improves the efficiency and reliability of ambiguity resolution. Furthermore, the proposed method suppresses the influence of outliers and enhances the robustness of the filtering process by utilizing the variational Bayesian filter based on the T-distribution. Experimental results demonstrate that, under the same filtering model, the proposed four-frequency combined observation ambiguity resolution model significantly improves the ambiguity fixing rate and positioning accuracy compared to the non-combined ambiguity resolution model. Moreover, the adoption of the variational Bayesian filter based on the T-distribution increases the ambiguity fixing rate by 3.7% and improves the positioning accuracy of the three components by 41.7%, 55.3%, and 40.6%, respectively, compared to the traditional Kalman filter algorithm. These findings validate the applicability of the proposed algorithm for high-precision dynamic relative positioning.

REFERENCES

[1] S. Guo, H. Cai, and Y. Meng, "BDS-3 RNSS technical characteristics and service performance," *Acta Geodadaetica et Cartographica Sinica*, vol. 48, no. 7, pp. 810–821, 2019.

[2] Z. Zhang, B. Li, X. He, Z. Zhang, and W. Miao, "Models, methods and assessment of four-frequency carrier ambiguity resolution for BeiDou-3 observations," *GPS Solutions*, vol. 24, no. 4, p. 96, Oct. 2020.

[3] X. Zhang and X. He, "Performance analysis of triple-frequency ambiguity resolution with BeiDou observations," *GPS Solutions*, vol. 20, no. 2, pp. 269–281, 2016.

[4] Y. Gao, Z. Lv, and P. Zhou, "Adaptive robust filtering algorithm for BDS medium and long baseline three carrier ambiguity resolution," *Acta Geodaetica et Cartographica Sinica*, vol. 48, no. 3, pp. 295–302, 2019.

[5] Y. Li, W. Yang, and H. Yan, "The optimal linear combination and characteristic analysis of BDS-3 multi-frequency signals," *J. Geodesy Geodynamic*, vol. 42, no. 6, pp. 612–615, 2022.

[6] M. Liu, C. Gao, and P. Shao, "Short baseline single-epoch positioning method of BDS-3 quad-frequency," *Sci. Surveying Mapping*, vol. 47, no. 11, pp. 17–24, 2022.

[7] X. Cao, J. Zhang, and C. Gao, "Research on BDS quad-frequency medium and long baseline ambiguity resolution," *J. Nanjing Univ. Inf. Sci. Technol. Natural Sci. Ed.*, vol. 16, no. 1, pp. 137–144, 2024.
[8] Z. Lv, Z. Wang, and J. Liu, "BDS-3 quad-frequency long baseline positioning algorithm considering ionospheric delay," *J. Bull. Surveying Mapping*, vol. 1, no. 4, pp. 71–78, 2023.
[9] J. Geng, J. Guo, X. Meng, and K. Gao, "Speeding up PPP ambiguity resolution using triple-frequency GPS/BeiDou/Galileo/QZSS data," *J. Geodesy*, vol. 94, no. 1, pp. 1–15, Jan. 2020.
[10] L. Liu, S. Pan, W. Gao, C. Ma, J. Tao, and Q. Zhao, "Assessment of quad-frequency long-baseline positioning with BeiDou-3 and Galileo observations," *Remote Sens.*, vol. 13, no. 8, p. 1551, Apr. 2021.
[11] Y. Huang, Y. Zhang, N. Li, Z. Wu, and J. A. Chambers, "A novel robust student's t-based Kalman filter," *IEEE Trans. Aerosp. Electron. Syst.*, vol. 53, no. 3, pp. 1545–1554, Jun. 2017.
[12] J. Li, Y. Yang, H. He, and H. Guo, "An analytical study on the carrier-phase linear combinations for triple-frequency GNSS," *J. Geodesy*, vol. 91, no. 2, pp. 151–166, Feb. 2017.
[13] G. Huang, B. Wang, and Y. Li, "Analysis of medium-long baseline single epoch ambiguity resolution based on BDS multi-frequency observations," *Sci. Surveying Mapping*, vol. 47, no. 12, pp. 33–38, 2022.
[14] J. Deng, A. Zhang, N. Zhu, and F. Ke, "Extra-wide lane ambiguity resolution and validation for a single epoch based on the triple-frequency BeiDou navigation satellite system," *Sensors*, vol. 20, no. 5, p. 1534, Mar. 2020.
[15] H. Zhai, L. Wang, and T. Cai, "Robust SLAM localization method based on improved variational Bayesian filtering," *J. Southeast Univ. English Ed.*, vol. 38, no. 4, pp. 340–349, 2022.
[16] H. Huang, J. Tang, C. Liu, B. Zhang, and B. Wang, "Variational Bayesian-based filter for inaccurate input in underwater navigation," *IEEE Trans. Veh. Technol.*, vol. 70, no. 9, pp. 8441–8452, Sep. 2021.
[17] K. Li, L. Chang, and B. Hu, "A variational Bayesian-based unscented Kalman filter with both adaptivity and robustness," *IEEE Sensors J.*, vol. 16, no. 18, pp. 6966–6976, Sep. 2016.
[18] Z. Wang and W. Zhou, "Robust linear filter with parameter estimation under student-t measurement distribution," *Circuits, Syst., Signal Process.*, vol. 38, no. 6, pp. 2445–2470, Jun. 2019.
[19] Z. Wang and W. Zhou, "Design and implementation of robust particle filter algorithms under student-t measurement distribution," *J. Electron. Inf. Technol.*, vol. 41, no. 12, pp. 2957–2964, 2019.
[20] C. Pan, J. Gao, Z. Li, N. Qian, and F. Li, "Multiple fading factors-based strong tracking variational Bayesian adaptive Kalman filter," *Measurement*, vol. 176, May 2021, Art. no. 109139.
[21] K. Wang, X. Li, and P. Wu, "A variational Bayesian modified unbiased converted measurement Kalman filter," *J. Chin. Inertial Technol.*, vol. 31, no. 3, pp. 261–267, 2023.
[22] S. Ji, W. Chen, C. Zhao, X. Ding, and Y. Chen, "Single epoch ambiguity resolution for Galileo with the CAR and LAMBDA methods," *GPS Solutions*, vol. 11, no. 4, pp. 259–268, Nov. 2007.

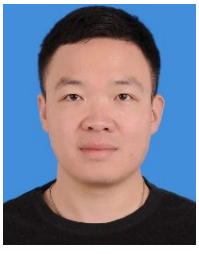

WEI CAI was born in Yichang, Hubei, China, in 1987. He received the B.S. degree in engineering from the Army Aviation Institute, in 2012. He is currently pursuing the master's degree in electronic information with the Institute of Geospatial Information, Information Engineering University, Zhengzhou, China.

From 2017 to 2021, he was an Engineer with Xi'an Mapping Terminus. His research interests include geodetic surveying and satellite navigation.

YANG SHEN received the bachelor's degree from the Institute of Surveying and Mapping, Information Engineering University, China, in 2022, where he is currently pursuing the Ph.D. degree. His current research interests include high-accuracy positioning and low-earth orbit satellite positioning methods.

MINGJIAN CHEN was born in Ürümqi, Xinjiang, China, in 1974. He received the B.S. and M.S. degrees in surveying and mapping engineering from Zhengzhou Institute of Surveying and Mapping, in 1996 and 2003, respectively, and the Ph.D. degree in control science and engineering from Northwestern Polytechnical University, in 2010. Since 2016, he has been a Professor with Information Engineering University. He has authored or coauthored more than 40 scientific articles. He is also an inventor of more than 20 patents and pending patents. His research interests include satellite navigation and multi-sensor integrated navigation.

WEI ZHOU was born in Zhongmu, Henan, China, in 1975. He received the B.S. degree in surveying and mapping from Information Engineering University, Zhengzhou, China, in 1998.

Since 2021, he has been a Professor of engineering with Xi'an Mapping Terminus. His research interests include geodetic surveying and satellite navigation.

JING LI was born in Minqin, Gansu, China, in 1983. She received the B.S. and M.S. degrees in engineering from Information Engineering University, in 2005 and 2013, respectively. From 2006 to 2010, she was an Assistant Engineer with Xi'an Mapping Terminus. Since 2014, she has been an Engineer with Xi'an Mapping Terminus. She mainly engaged in geodetic surveying and satellite navigation.

JIANLUN HE was born in Yancheng, Jiangsu, China, in 1993. He received the B.S. degree in automation and the M.S. degree in control science and engineering from the National University of Defense Technology, in 2015 and 2017, respectively.

He has been an Engineer with Xi'an Mapping Terminus, since 2018. His research interests include satellite navigation, integrated navigation, and geographical information systems.

XIN JING was born in Tianjin, China, in 1991. He received the B.S. degree in engineering from Information Engineering University, Zhengzhou, in 2014, and the M.S. degree in electronic information from the Institute of Geospatial Information, Information Engineering University, in 2023. From 2014 to 2020 and since 2023, he has been an Assistant Engineer with Xi'an Mapping Terminus. His research interests include geodetic surveying and satellite navigation.